batteries

MDPI

Article

Digital Twin-Enhanced Control for Fuel Cell and Lithium-Ion Battery Hybrid Vehicles

Xu Kang, Yujie Wang *, Cong Jiang and Zonghai Chen

Department of Automation, University of Science and Technology of China, No. 100 Fuxing Road, Hi-Tech Zone, Shushan District, Hefei 230027, China; kangxu0829@mail.ustc.edu.cn (X.K.); jiangcong@mail.ustc.edu.cn (C.J.); chenzh@ustc.edu.cn (Z.C.)

* Correspondence: wangyujie@ustc.edu.cn; Tel.: +86-1385-650-8387

Abstract: With the development of lithium-ion batteries and fuel cells, the application of hybrid power systems is becoming more and more widespread. To better optimize the energy management problem of fuel cell hybrid systems, the accuracy of system modeling and simulation is very important. The hybrid system is formed by connecting the battery to the fuel cell through an active topology. Digital twin technology is applicable to the mapping of physical entities to each other with high interactivity and fast optimization iterations. In this paper, a relevant model based on mathematical logic is established by collecting actual operational data; subsequently, the accuracy of the model is verified by combining relevant operating conditions and simulating the model. Subsequently, a three-dimensional visualization model of a hybrid power system-based sightseeing vehicle and its operating environment was established using digital twin technology to improve the model simulation of the fuel cell hybrid power system. At low speeds, the simulation results of the hybrid power system-based sightseeing vehicle have a small error compared with the actual running state, and the accuracy of the data related to each internal subcomponent is high. In the simple interaction between the model display vehicle and the environment, the communication state can meet the basic requirements of the digital twin model because the amount of data to be transferred is small. This study makes a preliminary attempt at digital parallelism by combining mathematical logic with visualization models and can be used as a basis for the subsequent development of more mature digital twin models.

Keywords: digital twin; fuel cell; hybrid power system; modeling and simulation

Citation: Kang, X.; Wang, Y.; Jiang, C.; Chen, Z. Digital Twin-Enhanced Control for Fuel Cell and Lithium-Ion Battery Hybrid Vehicles. *Batteries* **2024**, *10*, 242. https://doi.org/10.3390/batteries10070242

Academic Editor: Ottorino Veneri

Received: 6 June 2024
Revised: 30 June 2024
Accepted: 3 July 2024
Published: 5 July 2024

1. Introduction

1.1. Background and Motivation

New energy vehicles are receiving more and more attention because of their environmental friendliness and high efficiency. In recent years, automobile companies such as Honda and Mercedes-Benz have begun to focus on the development of electric vehicle technologies [1]. Battery Electric Vehicles (BEVs) are suitable for short distances [2]. Pure electric vehicles, due to the life limitations of existing batteries, face some problems in terms of recyclable technology, safety, and reliability [3]. A fuel cell (FC) is considered a zero-emission energy source since it does not produce tailpipe pollutants [4,5]. Proton-exchange membrane fuel cells (PEMFCs) are considered to be candidates for long-range FC vehicles due to their high power density, low greenhouse gas emissions, high efficiency, and relatively low operating temperature and pressure [6,7]. However, relying solely on stand-alone PEMFCs leads to a shorter system life cycle because the PEMFC system consumes all of the dynamic current [8]. Therefore, to compete with conventional technologies, it is necessary to reduce the cost of FC automotive powertrains and to improve their durability [9,10]. The disadvantage of PEMFCs is their slow dynamic response, which necessitates limiting their current slopes in order to prevent fuel shortages. Using PEMFCs as the primary

energy source with a battery as the secondary energy source to form a hybrid power system (HPS) can improve system performance and extend the system life [11,12]. The HPS not only is environmentally friendly but also has the potential to be highly efficient. With the development of FC hybrid vehicles, modeling simulation and management strategies for the HPS are crucial.

A digital twin (DT) is a versatile technological concept that has been introduced and quickly advanced in recent years, finding applications across numerous domains. Lim et al. provide a comprehensive overview of the DT concept and the associated technologies throughout its life cycle [13]. With the rise of the Industrial Internet of Things, the concept of the DT has expanded and evolved, moving from theoretical discussions to practical applications and drawing increased interest. Wang et al. examined the existing research on DT definitions and evaluated the distinctions among them [14]. In the manufacturing sector, DTs are integrated with shop floor designs and process production. A prime example is the cyber-physical production system, which serves as a fundamental and essential component of smart manufacturing [15]. DT-driven methods facilitate fault prediction and health management, establishing a novel framework for equipment health management [16]. Beyond the previously mentioned areas, DTs are utilized in computer numerical control machine tools, healthcare, urban management, environmental protection, and the automotive and construction sectors, showcasing considerable application potential [17–20]. Additionally, DT technology has enhanced research and applications in power equipment and smart manufacturing [21,22].

1.2. Contributions and Innovation Points

For the control of an HPS, the key lies in the management of multiple energy sources and power distribution. The most important part of the HPS is the FC, which is characterized by poor dynamic performance, good steady-state performance, complicated control, and a high level of danger. As a high-precision, hazardous energy source, FCs cannot be directly experimented on and tested with complex strategies. In this study, a digital-parallel framework for HPS modeling is proposed to target the problems of slow model data updates, a single available information source, and poor visualization in current HPS management. The framework utilizes the latest DT concept and related technologies to synchronize the operation of the cloud platform and the actual vehicle system through the interaction between the physical and software levels. This technology supports data interoperability between HPS and operational environment models in an integrated management platform. By reducing modeling complexity and enhancing data visualization, it enables data interoperability and display, marking a fundamental step toward achieving a higher level of DT and simulation.

1.3. Section Arrangement

The remainder of this paper is organized as follows: Section 2 describes the model-building process and the structure of the DT framework, while Section 3 outlines the process of using this modeling approach with case demonstrations. Section 4 serves as the conclusion, providing a summary description of the study. In Section 5, experimental studies under different operation conditions are presented to verify the effectiveness of the proposed method.

2. The Architecture of the DT for the HPS

DTs are constructed in a variety of ways, and the results obtained possess different characteristics. In this study, the focus is on the electrical properties of the HPS as well as the characterized external properties. Therefore, it is necessary to characterize the external and internal structures of the FC as well as the lithium-ion battery. On the external side, the FC system consists of an FC stack comprising cathode and anode plates with a proton-exchange membrane, along with some auxiliary systems: an air compressor, a hydrogen circulation pump, a pressure control system, a temperature control system, and a water control system.

The FC stack is composed of 23 monolithic FCs, and the relevant FC electrical characteristics are obtained from the polarization curves and efficiency curves. On the other hand, the lithium-ion battery is a battery pack formed by combining 20 monolithic cells using a 20-series, 1-parallel structure, in addition to the utilization of a battery management system for management.

Subsequently, the behavioral model simulation of the HPS is carried out, as shown in Figure 1, using a real-time computer to run the model. As for the DT model construction, the external parameters and connection structure required for the 3D model, as well as the operational data of the behavioral model, are obtained through a hardware-in-the-loop test between the real-time computer and the actual physical system. In this study, an online 3D scene editor based on three.js is used as the engine to build the visualization model. Then, a data-driven approach is used to synchronize the running data with the DT to achieve the construction of the DT model on the server side. On the basis of real-time communication, the DT model is run to obtain enhancement parameters, which are used as inputs for platform and algorithm enhancement to achieve better results. In this study, the augmented data are used for speed prediction, working condition identification, and classification, and further, FC life decay is taken into account to facilitate the design of energy management strategies in the future.

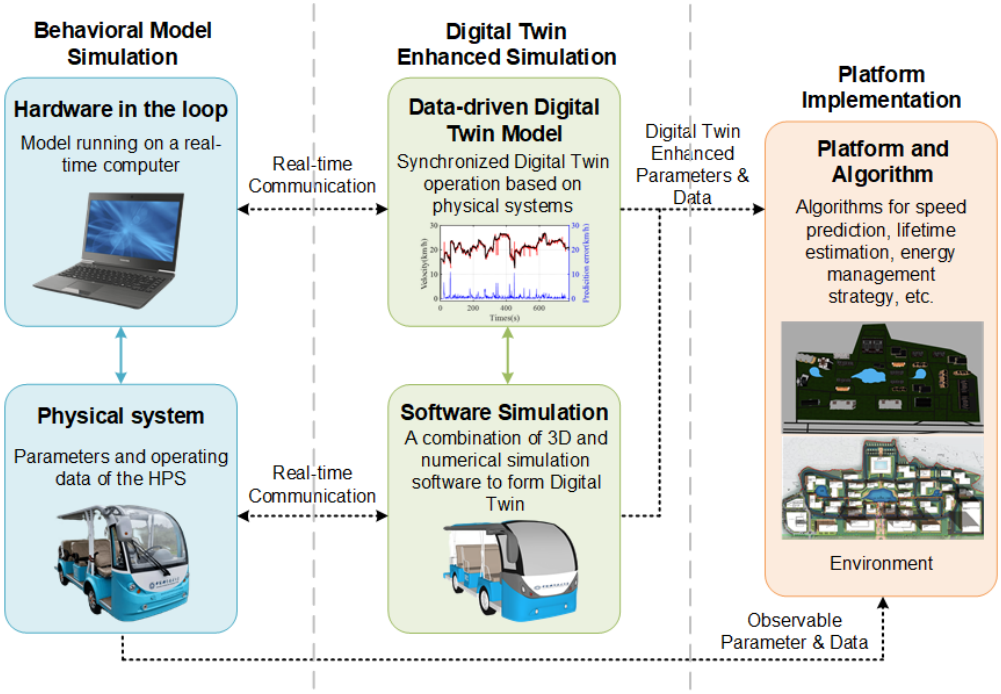

Figure 1. Digital twin simulation flow architecture.

3. The Structure of the Edge-to-Cloud HPS Management System

According to the research by Tao et al., the current maturity levels of DTs are classified as follows: L0 involves using the DT model to describe and depict the physical entity; L1 entails utilizing the DT model to replicate the real-time state of and changes in the physical entity; L2 involves the DT model indirectly controlling the physical entity's operations; L3 uses the DT model to forecast the future state and operational processes of the physical entity; L4 optimizes the physical entity using the DT model; and L5, during long-term synchronized operation, allows for autonomous twinning through dynamic reconfiguration, spanning the entire life cycle [23]. Unlike Tao's study, this research categorizes the advancement levels of the DT based on the sequence of interactions between the actual operating system and the DT model into the following categories: Digital backward: The DT model is run after the actual system is run, and the operational data of the actual system are used for simulation. Digital parallel: The DT model and the actual system are run

synchronously, and the simulation process obtains both the actual operational data and the simulation data generated by the DT model. Digital first: The results of the DT model in the virtual environment are used to realize future guidance and prediction of the actual system, as well as fault and risk avoidance. Therefore, after the mechanistic modeling and simulation of the HPS, this study explored the concepts of digital backward and digital parallelism. The specific performance lies in the 3D modeling and remote data acquisition of the HPS, and a cloud-based platform was built to realize the construction and display of a DT.

As shown in Figure 2, this intelligent edge-to-cloud HPS management system consists of five layers: the first layer is the physical system layer, which contains components such as motors, lithium-ion battery packs, FC stacks, hydrogen tanks, and air compressors, which work together to convert, store, and generate electrical energy. The energy flow starts from the hydrogen tank and the air compressor, which transfers hydrogen and oxygen to the FC stack for reaction, which is connected to the lithium-ion battery pack via unidirectional DC/DC to form the HPS, a hybrid power source that connects to the electric motor via AC/DC to drive the vehicle. The physical system layer is the base of the system and the source from which we obtain information about the HPS. The second layer is the smart sensing terminal layer, where the battery management system, smart sensors, and FC management system realize data exchange through efficient 5G and CAN transmission to monitor and control the system operation status in real time, specifically through the circuit voltage detector, temperature, and pressure integrated sensor and air meter for data sensing and detection. In this layer, the CAN communication baud rate is 250 kb/s. In order to reflect the error between the simulation results and the actual system in a more direct way, the data collected by the hardware system is not pre-processed by noise filtering and so on. The next layer is the data space layer, which realizes the public cloud, private cloud, database, data analysis, and data security. This layer provides extensive data storage, management, and security functions for the system. Further up is the platform layer, which provides development and simulation environments, including a development platform, a DT environment, and a DT model of the FC vehicle to support further development and optimization of the system. The topmost layer is the application layer, which includes model derivation, adaptive parameter calibration, and prediction and control. Model derivation constructs the mathematical model of the system through actual data and simulation results, adaptive parameter calibration adjusts the system parameters based on real-time data, and prediction and control realize the intelligent prediction and precise control of the physical system through these models and data. Overall, the various layers of this system collaborate to form a powerful intelligent edge-to-cloud HPS management platform capable of realizing efficient and intelligent energy conversion and utilization.

The platform adopts various technical means to facilitate two-way interaction and feedback between the physical layer and the cloud, enriching the ways and means of realizing DT models. This exploration also lays the foundation for the subsequent realization of digital first and the exploration of more possibilities of DT technology. When dealing with a complex physical entity with multiple components, such as an HPS, it is necessary to analyze its mathematical relationships and model its mechanisms. It is also necessary to collect a large amount of data, analyze its structural composition and operating scenarios, and update the model accordingly. The visualization function of the DT makes it easy for users to gain an intuitive and clear understanding of it. Simulation activities, such as model-based analyses, experimentation, and training, can ensure that the DT virtual system corresponds to the physical system for accurate mapping. The obtained simulation results can also be used to evaluate, diagnose, and control the real system.

In the model-building phase, DT involves various modeling and simulation techniques. The primary aspect of this technique includes modeling a physical system using simulation tools and constructing a virtual system in digital space that closely resembles the real system. This phase is referred to as the 'digital backward' phase, in which the transition from the physical layer to the level of the virtual digital model is achieved after

obtaining the operational state of the physical object in question and the correlation of the relevant subsystems. This description can include one or more of the geometrical, physical, behavioral, and rule aspects. The dimension describes the properties and characteristics of one or more aspects of the physical entity, thus allowing it, to some extent, to replace the physical entity for simulation analysis or experimental verification. As can be seen from the procedure, in the digital-backward stage, the first thing that needs to be realized is the acquisition of the parameters of the module components, as well as the operational data. After obtaining the relevant parameters, the virtual digital model of the module components can be further established, and the combination of the components can be coordinated to establish the system model.

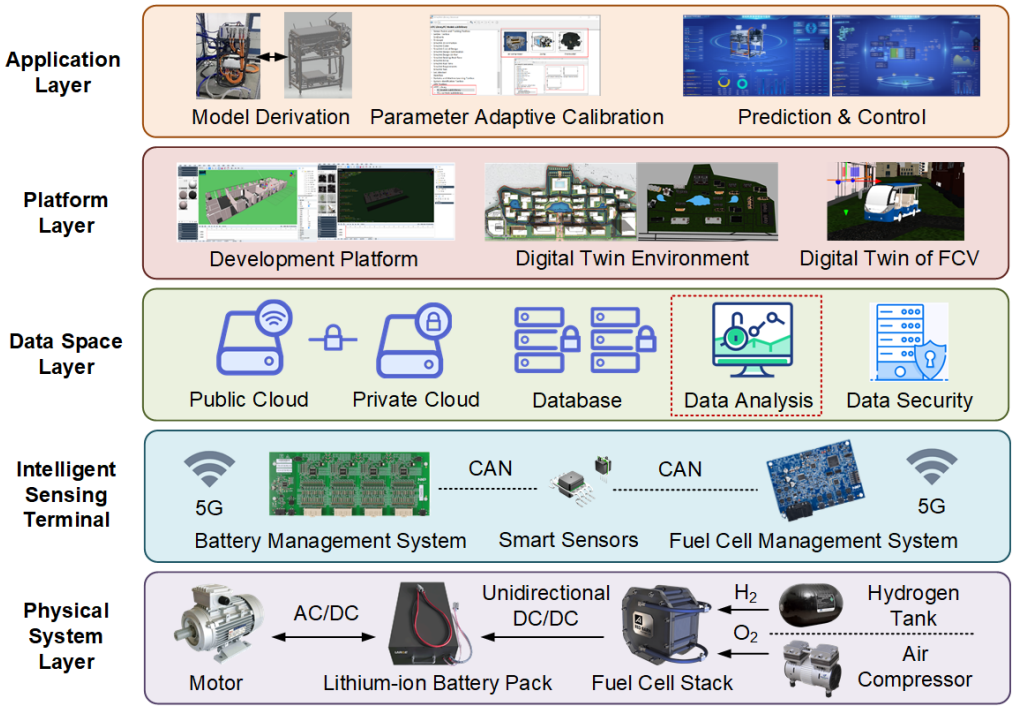

Figure 2. The structure of the edge-to-cloud HPS management system.

The digital-parallel phase was attempted in this study, where the DT model runs synchronously with the physical entity. In this phase, the same operational state and process as the physical entity are presented synchronously and intuitively, and the outputs are compared with the physical entity. The relevant results will be analyzed in the following sections. In this study, the relevant parameters of each module are captured and reflected in real time on the host computer during vehicle operation, which allows for the remote monitoring of the physical entity to a certain extent.

4. Digital-Parallel-Enhanced HPS Management

4.1. DT Model for HPS

To establish the DT model, the first step is to develop the HPS mechanism model. The HPS structure and its model-building process are described as follows. The vehicle's power system features an FC linked to a DC/DC converter, which, together with the battery, connects to an electric motor to drive the vehicle. The FC and battery are chosen as the power sources for the hybrid vehicle's motor. DC/DC converters facilitate connections between the FC and battery sides and the motor side, and their efficiency is evaluated through actual operation tests.

To determine the total power needed for the vehicle, the vehicle power balance equation shown in Equation (1) is used:

$$P_{\mathrm{re}} = (fMg + \frac{1}{2}\rho_a \mathrm{A} C_D v^2 + Ma)v \tag{1}$$

where f is the rolling resistance coefficient, set at 0.02; M is the overall vehicle mass; g represents gravitational acceleration; ρ_a is the air density, set at 1.2; A denotes the vehicle's windward area; C_D is the drag coefficient; a signifies the vehicle's acceleration; and v stands for the vehicle speed.

To account for the electrical characteristics of the lithium-ion battery, the Rint model is utilized, representing the battery with an open-circuit voltage and internal resistance connected in series, as illustrated in Equation (2) below:

$$V_{\mathrm{bat}} = U_{\mathrm{ocv}} + I_{\mathrm{bat}} R_{\mathrm{bat}} \tag{2}$$

where V_{bat} represents the terminal voltage of the battery, U_{ocv} represents the open-circuit voltage of the battery, I_{bat} represents the output current of the battery, and R_{bat} represents the internal resistance of the battery.

To simplify calculations, a constant is used to represent both the charge resistance and discharge resistance, as their values are nearly identical within a specific state-of-charge (SOC) range. The SOC of the battery is represented by Equation (3) below:

$$\mathrm{SOC} = \frac{\mathrm{Q}_0 - \int_0^{\mathrm{t}} \mathrm{I}_{\mathrm{bat}}(\mathrm{t})\mathrm{dt}}{\mathrm{Q}_{\mathrm{max}}} \tag{3}$$

where Q_0 indicates the initial capacity of the battery, and Q_{max} indicates the maximum capacity of the battery.

To model the FC, only its external characteristics, such as the current, voltage, hydrogen consumption, and efficiency, are considered. A commonly used FC expression is shown in Equation (4), which describes an empirical model that has been repeatedly summarized and validated:

$$\begin{aligned} V_{\mathrm{FC}} =& U_{\mathrm{FC}} - R_{\mathrm{ohm}} \cdot (i_{\mathrm{FC}} + i_n) \\ & - A\ln(\frac{i_{\mathrm{FC}} + i_n}{i_0}) - B\ln(1 - \frac{i_{\mathrm{FC}} + i_n}{i_0}) \end{aligned} \tag{4}$$

In this model, U_{FC} is the open-circuit voltage of the FC, V_{FC} is the output voltage, i_{FC} is the output current, R_{ohm} represents the internal resistance, and A, B, i_0, and i_n are relevant empirical parameters.

In the operation of the FC, i_n and i_L have negligible effects on the FC's input voltage and are also challenging to measure. As a result, these terms can be omitted, which simplifies the equation to Equation (5):

$$V_{\mathrm{FC}} = U_{\mathrm{oc}} - R_{\mathrm{ohm}} \cdot i_{\mathrm{FC}} - Alni_{\mathrm{FC}} + Me^{Ni_{\mathrm{FC}}} \tag{5}$$

where $U_{\mathrm{oc}} = U_{\mathrm{FC}} + A\ln(i_0)$, and M and N are given as constants.

The rate of hydrogen consumption in the FC's chemical reactions can be described by Equation (6):

$$\dot{m}_{\mathrm{FC}_{\mathrm{H}_2}} = \frac{NM_{\mathrm{H}_2} i_{\mathrm{FC}}}{nF} \tag{6}$$

In this equation, N represents the number of FC monomers, n denotes the number of electrons transferred during the reaction, F is the Faraday constant, which equals 96,487 C/mol, and M_{H_2} is the molar mass of hydrogen, which is 2.02 g/mol.

Then, the external parameters are obtained for the relevant external subcomponent structure for 3D visualization model construction. In this study, the aforementioned edge-to-cloud platform is used for the construction of the DT model. The shape, appearance, size, location, and connection mode of the design subcomponents are first obtained from

the physical layer and then imported to the DT layer through the communication layer. In the DT layer, it is necessary to first obtain the actual operating environment of the vehicle and then construct the environment base for the DT model. Subsequently, the built DT subcomponents are combined and arranged to form an interactive DT model. Then, the external parameters are obtained for the relevant external subcomponent structure for 3D visualization model construction. In this study, the aforementioned edge-to-cloud platform is used for the construction of the DT model. The shape, appearance, size, location, and connection mode of the design subcomponents are first obtained from the physical layer and then imported to the DT layer through the communication layer. In the DT layer, it is necessary to first obtain the actual operating environment of the vehicle and then construct the environment base for the DT model. Subsequently, the built DT subcomponents are combined and arranged to form an interactive DT model.

4.2. Speed Prediction for HPS Management

The effectiveness of the HPS DT platform is also demonstrated by the prediction of the operational state of the vehicle model. In this study, a Markov chain prediction method is used to predict the future operating speed of the vehicle. The basic principle of Markov prediction is described below, where the time during the velocity change is discretized as $n = 0, 1, 2, \ldots$, and the possible velocity states are denoted by the state space $X_n = 1, 2, \ldots, k$, denoting the k possible states that the velocity may be in. If the value of X_{n+1} depends on the value of X_n and the transfer probability, independent of the previous values of $x_{n-1}, x_{n-2}, \ldots$, then this is called the process of transferring discrete states according to time a Markov chain. $a_i(n) = P(X_n = i)$ denotes the state probability and satisfies Equation (7):

$$\sum_{i=1}^{k} a_i(n) = 1, n = 0, 1, 2, \ldots \tag{7}$$

The probability of going from $X_n = i$ to $X_{n+1} = j$ is denoted by the transfer probability $P_{ij} = P(X_{n+1} = j | X_n = i)$. $P = \left(P_{ij}\right)_{k \times k}$ denotes the state transfer probability matrix, or transfer matrix for short, which satisfies Equations (8) and (9):

$$P_{ij} \geq 0, i, j = 1, 2, \ldots, k \tag{8}$$

$$\sum_{j=1}^{n} p_{ij} = 1, i, j = 1, 2, \ldots, k \tag{9}$$

In the above formulation, the state transfer probability matrix for each of the two stages is the same matrix P. This property is called the time-aligned nature of the Markov chain.

Firstly, the state space is determined based on the historical vehicle speeds obtained from actual measurements. Then, state division is performed to obtain the state transfer probability matrix between states. The subsequent prediction is based on this, and the current speed is used as the initial state to predict the future state. In order to meet the requirements for speed prediction accuracy and the speed of historical data collection, the prediction lengths were set to 1 s, 3 s, and 5 s. Ideally, the shorter the required sliding window is, the faster the prediction speed is, and 10 s was chosen as the sliding window length in this study. The obtained prediction results are shown in Figure 3, where (a), (b), and (c) are the prediction results for prediction lengths of 1 s, 3 s, and 5 s, respectively, from which it can be seen that when the prediction length is gradually increased, the prediction accuracy also decreases. When it reaches 5 s, the prediction accuracy decreases significantly. Based on the prediction results, a prediction length of 3 s was chosen.

In this study, the actual vehicle operating speed was collected and predicted for the vehicle, which is a park vehicle and maintains a speed of 25 km/h or less. After experimentation, it was found that a better prediction result could be achieved using 10 s, so this window length was chosen for prediction. With the help of the edge-to-cloud HPS management system, the speed data obtained in actual operation can be updated

regularly for the state transfer probability matrix. This updating is conducive to improving the accuracy of the prediction, reducing the prediction delay, and effectively obtaining a dynamic response when the driving conditions change.

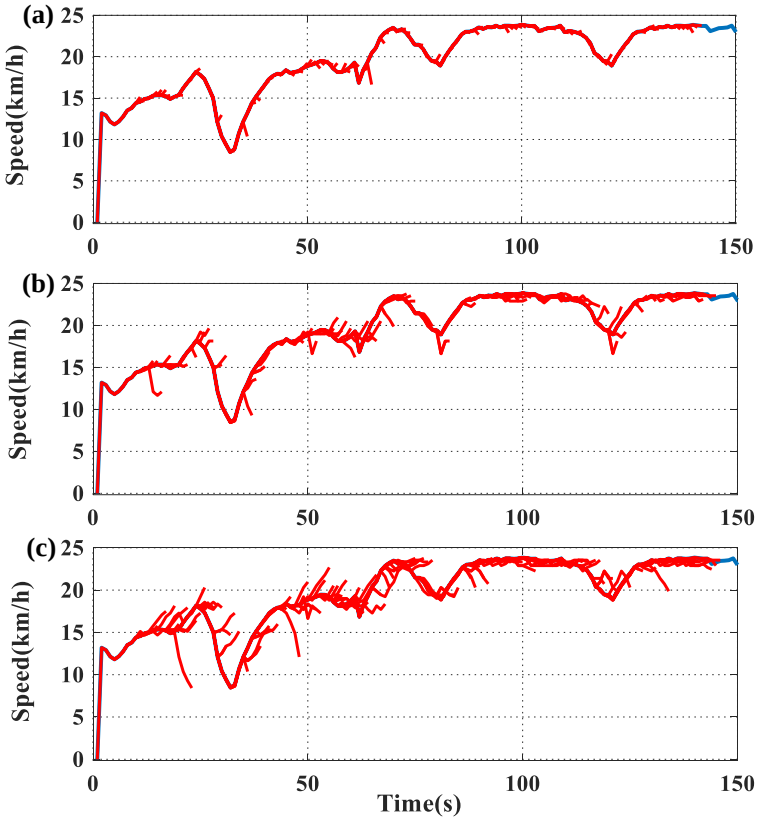

Figure 3. Speed prediction results. (**a**) Vehicle speed prediction results for a prediction step of 1 s; (**b**) Vehicle speed prediction results for a prediction step of 3 s; (**c**) Vehicle speed prediction results for a prediction step of 5 s.

4.3. Edge-to-Cloud HPS Energy Management

In this section, a case study on how to implement edge-to-cloud HPS energy management is presented. As mentioned in the previous subsection, this study used park vehicles for the operation and data collection of the actual system. The parameters of each energy source are collected through sensors for state estimation. In the next step, the obtained data are transmitted to the DT platform through communication means such as 5G and stored in the cloud database. The DT platform performs model validation and synchronization by performing model virtual mapping through the previously created model. Then, digital parallelism is utilized to perform speed prediction and the DT model update in the actual system operation. After obtaining the DT model and speed prediction results of the HPS, the energy management and power allocation of the HPS are performed by the edge-to-cloud HPS management system proposed in this paper. The system integrates and fuses various technologies to bridge the whole process of information acquisition, data communication, model operation, and real-time application from hardware to software. The specific links in the system for energy management are shown in Figure 4.

The constraints of the proposed rule-based energy management strategy in this study are given in the following Equation (10):

$$\begin{cases} 0 \le SOC \ge 1 \\ -10kW \le P_b \ge 10kW \\ 0kW \le P_FC \ge 5kW \end{cases} \tag{10}$$

The operating rules for all rule-based energy management strategies are as follows.

In state 1, the FC is in the start-up phase. During this phase, the entire power demand is met by the lithium-ion battery system while the FC system is initiated. The relationship between the system's power requirements can be represented by Equation (11):

$$\begin{cases} P_{FC} = 0 \\ \eta_b P_b = P_{start} + P_{load} \\ P_{re} = \eta_{ac} P_{load} \end{cases} \tag{11}$$

In this context, P_{FC} denotes the power output of the FC, P_{start} refers to the power required to start up the FC, P_{load} indicates the power required by the load, P_{re} represents the power for the vehicle's motor, P_b signifies the power from the battery, η_b is the efficiency of the battery's bidirectional converters, and η_{ac} denotes the efficiency of the DC/AC inverter.

State 2 represents the FC Stand-Alone Mode. During this state, if the SOC of the battery falls below a predefined lower threshold, the FC will take over the power supply and charge the battery, providing all the required power for the system. The power relationship in this mode can be expressed by Equation (12):

$$\begin{cases} \eta_{FC} P_{FC} = P_{load} + \eta_b P_b \\ P_{re} = \eta_{ac} P_{load} \end{cases} \tag{12}$$

where η_{FC} represents the efficiency of the converter of the FC system.

Set state 3: Battery-Independent Operation Mode. When the power demand is lower than the minimum output power of the FC, the FC will cease operation, and all the required power will be provided by the battery system. The system power relationship can be expressed as Equation (13):

$$\begin{cases} P_{FC} = 0 \\ \eta_b P_b = P_{load} \\ P_{re} = \eta_{ac} P_{load} \end{cases} \tag{13}$$

State 4 describes the FC + Battery Operating Mode. In this state, if the SOC of the battery drops below the lower limit, the FC takes over to charge the battery while simultaneously supplying all the demanded power to the system. The power balance in this mode is given by Equation (14):

$$\begin{cases} \eta_{FC} P_{FC} + \eta_b P_b = P_{load} \\ P_{re} = \eta_{ac} P_{load} \end{cases} \tag{14}$$

Additionally, the lithium-ion battery system is designed to recover braking energy when the SOC of the battery is below its upper threshold. Energy recovery ceases when the SOC exceeds this upper limit.

In this study, 1500 s was selected for validation in the park vehicle's operating conditions, and the optimization objective was set to minimize HPS consumption. The energy management of the vehicle HPS will be performed mainly for FC as well as lithium-ion battery power allocation. The predictions will be smoothed as a subsequent trend of the real-time speed and synchronized with the currently running DT model. The method has better performance in the selected operating conditions, which can meet the power demand of the vehicle and also ensure a smoother FC operation.

The system increases the breadth of input information by virtually mapping the model on the basis of data obtained from the actual vehicle operation. The data processing speed on the DT platform is faster, and it can also determine the trend of the actual vehicle operation status in advance. The edge-to-cloud HPS energy management system proposed in this study improves the fast-tracking capability of the virtual model on the basis of digital parallelism, improves the effectiveness of the energy management strategy, and enhances

the timeliness of the system control. In addition, the DT platform allows subsequent real-time monitoring and warning of abnormal vehicle states.

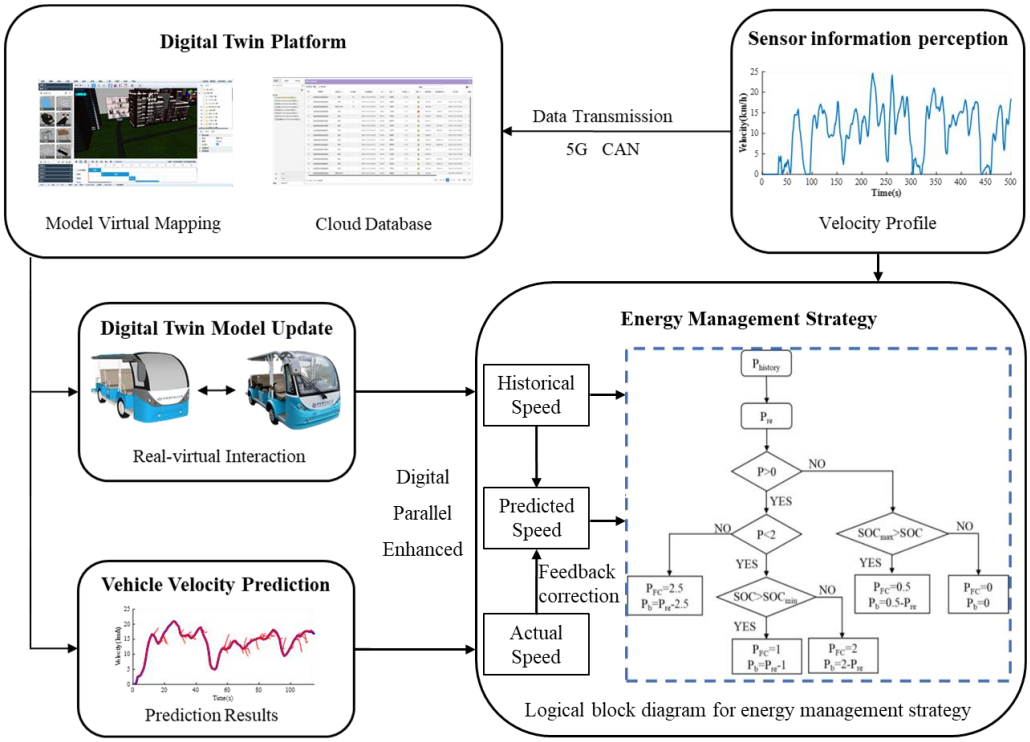

Figure 4. HPS control process with digital parallel.

5. Results and Discussion

In order to obtain the accuracy and fast-tracking capability of the model, the hybrid powertrain trolley was experimentally validated in this study. As shown in Figure 5, the DT model operation results include the results of running the physical vehicle, the DT model simulation results, and the HPS subsystem simulation results.

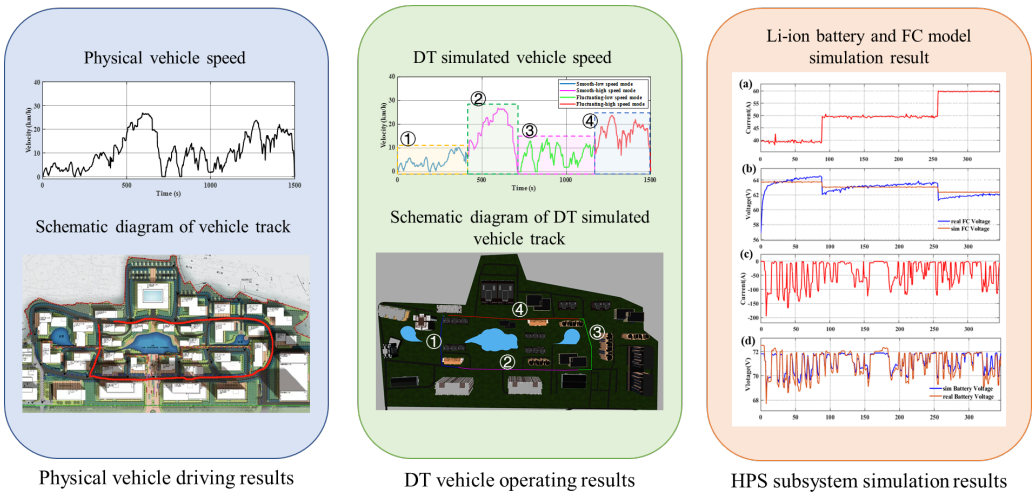

Figure 5. DT model simulation results.

The physical vehicle operation results include the vehicle's driving speed profile and the physical vehicle's driving track map in the park. The DT vehicle simulation results obtained on the DT platform show that the DT platform divides the complete driving speed profile into four speed modes with different characteristics, including smooth low-speed mode, smooth high-speed mode, fluctuating low-speed mode, and fluctuating

low-speed mode. They correspond to four different sections of the park, indicating the fast-tracking capability of the DT model. In addition, during vehicle operation, the vehicle route recorded by the DT model closely matches the actual vehicle route with a high degree of visualization. It enables communication and display from the cloud with little or no impact on the vehicle's energy consumption and prepares the groundwork for the subsequent display of more detailed information in the 3D model. The final HPS subsystem simulation results are analyzed by comparing the actual operating data of the lithium-ion battery and FC with the model simulation data. This analysis refers to the dynamic characteristics of the battery and FC for state estimation, and a short-time experimental test with a duration of 300 s was conducted on a real vehicle. The obtained voltage and current curves of the FC and the voltage and current curves of the battery model are shown in (a), (b), (c), and (d). By analyzing the error, it can be concluded that the driving path of the DT vehicle is basically consistent with the driving path of the actual system, and the model simulation results are within a reasonable range. The working condition classification results are very consistent with the driving path. The FC model has a large error in the start-up phase, which can reach 10%, and the error in the regular operation phase is within 3%. The error of the battery model in the whole process stage is within 1.5%.

In order to validate the case flow of HPS energy management, we conducted a 1500 s long-time experimental test on a real vehicle. The digital-parallel operation of the HPS under the experimental conditions yielded the following relevant operational results: by analyzing the power distribution results, it can be concluded that the FC operation is more stable, the power fluctuation is very small, and the battery is able to complete the energy recovery. In addition, Figure 6 illustrates the energy management strategies under the same operating conditions with different upper and lower SOC limit rulemaking. The output power of the lithium-ion battery and the FC, the hydrogen consumption, and the variation in the battery SOC are analyzed and compared. During vehicle operation, a positive lithium-ion battery power indicates that the lithium-ion battery is discharged, and a negative lithium-ion battery power indicates that the FC charges the lithium-ion battery. In order to fully utilize the lithium-ion battery, the SOC interval is set to be greater than or equal to 40% of the battery pack capacity, the lower limit is set in the range of (0.3–0.5), and the upper limit is set in the range of (0.8–0.9).

Figure 5a shows the vehicle power demand and the output power curve of the lithium-ion battery with the FC when the SOC operation range is set to (0.3–0.8), and (b) and (c) indicate the hydrogen consumption and the change in battery SOC under this SOC range, respectively. The SOC ranges within (0.4–0.9) in Figure 6d–f and (0.5–0.9) in Figure 6g–i, where P_{re} denotes the vehicle power demand, P_b denotes the lithium-ion battery output power, and P_{FC} denotes the FC output power. After analyzing the strategy results, as shown in Table 1, a conclusion can be drawn.

Table 1. Performance comparison of the rule-based energy management strategies with different SOC ranges.

SOC Range (%)	H_2 Consumption (g)	ΔSOC (%)	FC Lifetime Decay (%)
(0.3–0.8)	36.05	29.08	3.56
(0.4–0.9)	33.24	20.35	3.89
(0.5–0.9)	27.32	6.67	3.91

According to the table, it can be seen that the current SOC setting significantly reduces hydrogen consumption while sacrificing some of the FC life decay rate and ensuring that the SOC varies within a small range, improving the fuel use efficiency and sustainability of vehicle operation. When the upper and lower SOC limits were set to 0.5 and 0.9, respectively, the energy management strategy had the lowest hydrogen consumption and the best SOC maintenance.

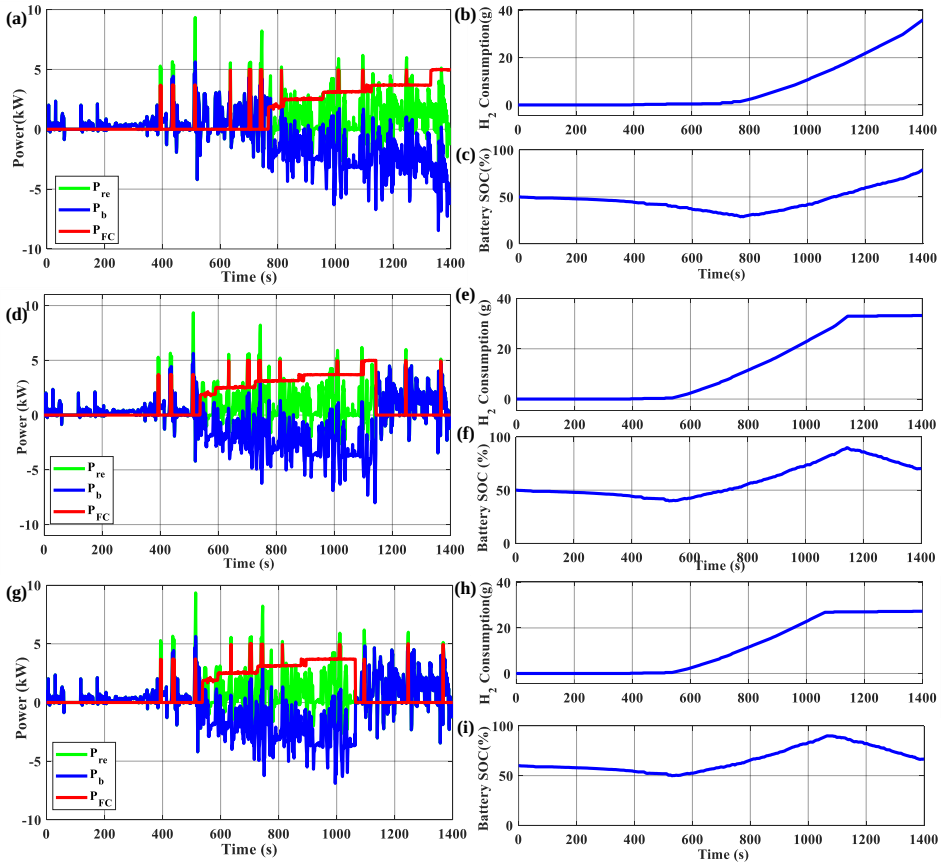

Figure 6. Rule-based energy management strategy results using the DT platform. (**a**) Vehicle demand power curve, fuel cell and battery output power curves for the soc range setting of (0.3–0.8); (**b**) Hydrogen consumption curve for the soc range setting of (0.3–0.8); (**c**) SOC change curve for the soc range setting of (0.3–0.8); (**d**) Vehicle demand power curve, fuel cell and battery output power curve for the soc range setting of (0.4–0.9); (**e**) Hydrogen consumption curve for the soc range setting of (0.4–0.9); (**f**) SOC change curve for the soc range setting of (0.4–0.9); (**g**) Vehicle demand power curve, fuel cell and battery output power for the soc range setting of (0.5–0.9); (**h**) Hydrogen consumption curves for soc range settings of (0.5–0.9); (**i**) SOC change curves for soc range settings of (0.5–0.9).

6. Conclusions

To enhance the modeling accuracy and simulation effect of the HPS, a digital-parallel-based HPS energy management system is used in this study. First, the actual physical parameters of the FC vehicle are analyzed. A mechanism model is then established, incorporating the operation mechanism and collected data. Subsequently, the vehicle and its operational environment are modeled in a three-dimensional simulation. Following this, relevant data from sensors are gathered, and vehicle speed prediction is executed.

After obtaining these results, a digital parallel is achieved through the utilization of a DT platform, allowing the real-time execution of both the actual vehicle model and its virtual counterpart. This process enriches the information available for energy management. This study represents an initial exploration of the digital parallel and visualization model. It serves as a foundational study for the subsequent development of more sophisticated DT models.

It is important to note that this digital parallelism was specifically tested within the context of an HPS, but the methodology can be adapted to various application areas. Furthermore, the implementation of digital-backward marching is integrated into this approach. Consequently, this study provides an innovative perspective for the model

validation of complex systems through multi-repetition experiments, particularly for high-risk systems.

Author Contributions: Conceptualization, X.K. and Y.W.; methodology, writing—original draft preparation, X.K.; software, C.J.; visualization, X.K. and C.J.; resources, writing—review and editing, and analysis, Y.W.; supervision, Z.C. All authors have read and agreed to the published version of the manuscript.

Funding: This work was supported by the National Natural Science Foundation of China (Grant No. 62373340).

Data Availability Statement: The data presented in this study are available on request from the corresponding author. The data are not publicly available due to this data relates to company-related information.

Conflicts of Interest: The authors declare no conflicts of interest.

References

1. Zhou, L.; Zheng, Y.; Ouyang, M.; Lu, L. A study on parameter variation effects on battery packs for electric vehicles. *J. Power Sources* **2017**, *364*, 242–252. [CrossRef]
2. Alves, J.; Baptista, P.C.; Gonçalves, G.A.; Duarte, G.O. Indirect methodologies to estimate energy use in vehicles: Application to battery electric vehicles. *Energy Convers. Manag.* **2016**, *124*, 116–129. [CrossRef]
3. Sockeel, N.; Ball, J.; Shahverdi, M.; Mazzola, M. Passive Tracking of the Electrochemical Impedance of a Hybrid Electric Vehicle Battery and State of Charge Estimation through an Extended and Unscented Kalman Filter. *Batteries* **2018**, *4*, 52. [CrossRef]
4. Lü, X.; Miao, X.; Liu, W.; Lü, J. Extension control strategy of a single converter for hybrid PEMFC/battery power source. *Appl. Therm. Eng.* **2018**, *128*, 887–897. [CrossRef]
5. İnci, M.; Bayındır, K.C. Single-stage vehicular fuel cell system with harmonic elimination capability to suppress distortion effects of electric vehicle parking lots. *J. Power Sources* **2024**, *597*, 234175. [CrossRef]
6. Pollet, B.G.; Staffell, I.; Shang, J.L. Current status of hybrid, battery and fuel cell electric vehicles: From electrochemistry to market prospects. *Electrochim. Acta* **2012**, *84*, 235–249. [CrossRef]
7. Wang, Y.; Yang, X.; Sun, Z.; Chen, Z. A systematic review of system modeling and control strategy of proton exchange membrane fuel cell. *Energy Rev.* **2024**, *3*, 100054. [CrossRef]
8. Talaat, M.; Elgarhy, A.; Elkholy, M.H.; Farahat, M.A. Integration of fuel cells into an off-grid hybrid system using wave and solar energy. *Int. J. Electr. Power Energy Syst.* **2021**, *130*, 106939. [CrossRef]
9. Hu, X.; Jiang, J.; Egardt, B.; Cao, D. Advanced power-source integration in hybrid electric vehicles: Multicriteria optimization approach. *IEEE Trans. Ind. Electron.* **2015**, *62*, 7847–7858. [CrossRef]
10. İnci, M. Connecting multiple vehicular PEM fuel cells to electrical power grid as alternative energy sources: A Case Study. *Int. J. Hydrogen Energy* **2024**, *52*, 1035–1051. [CrossRef]
11. Ibrahim, A.; Jiang, F. The electric vehicle energy management: An overview of the energy system and related modelling and simulation. *Renew. Sustain. Energy Rev.* **2021**, *144*, 111049. [CrossRef]
12. İnci, M.; Büyük, M.; Özbek, N.S. Sliding mode control for fuel cell supported battery charger in vehicle-to-vehicle interaction. *Fuel Cells* **2022**, *22*, 212–226. [CrossRef]
13. Lim, K.Y.H.; Zheng, P.; Chen, C.H. A state-of-the-art survey of digital twin: Techniques, engineering product lifecycle management and business innovation perspectives. *J. Intell. Manuf.* **2020**, *31*, 1313–1337. [CrossRef]
14. Wang, Y.; Xu, R.; Zhou, C.; Kang, X.; Chen, Z. Digital twin and cloud-side-end collaboration for intelligent battery management system. *J. Manuf. Syst.* **2022**, *62*, 124–134. [CrossRef]
15. Wang, P.; Luo, M. A digital twin-based big data virtual and real fusion learning reference framework supported by industrial internet towards smart manufacturing. *J. Manuf. Syst.* **2021**, *58*, 16–32. [CrossRef]
16. Wang, Y.; Kang, X.; Chen, Z. A survey of digital twin techniques in smart manufacturing and management of energy applications, *Green Energy Intell. Transp.* **2022**, *1*, 100014.
17. Wei, Y.; Hu, T.; Zhou, T.; Ye, Y.; Luo, W. Consistency retention method for cnc machine tool digital twin model. *J. Manuf. Syst.* **2021**, *58*, 313–322. [CrossRef]
18. Soumya, S.; Max, W.; Kai Peter, B. Implementation of Battery Digital Twin: Approach, Functionalities and Benefits. *Batteries* **2021**, *7*, 78. [CrossRef]
19. Liu, Y.; Xie, Q. Technical Characteristics of Digital Twins and Application Prospects in the Field of Flight Testing. *J. Syst. Simul.* **2021**, *33*, 1364–1373.
20. Jiang, F.; Ding, Y.; Song, Y.; Geng, F.; Wang, Z. Digital twin-driven framework for fatigue life prediction of steel bridges using a probabilistic multiscale model: Application to segmental orthotropic steel deck specimen. *Eng. Struct.* **2021**, *241*, 112461. [CrossRef]

21. Li, X.; He, B.; Zhou, Y.; Li, G. Multisource model-driven digital twin system of robotic assembly. *IEEE Syst. J.* **2021**, *15*, 114–123. [CrossRef]
22. Li, X.; Liu, X.; Wan, X. Overview of Digital Twins Application and safe Development. *J. Syst. Simul.* **2021**, *31*, 385–392.
23. Tao, F.; Zhang, Y.; Zhang, H. Digital twin maturity model. *Comput. Integr. Manuf. Syst.* **2022**, *5*, 28.